

Mode-Coupling Theory for Active Brownian Particles

Alexander Liluashvili,¹ Jonathan Onody,¹ and Thomas Voigtmann^{1,2}

¹*Institut für Materialphysik im Weltraum, Deutsches Zentrum für Luft- und Raumfahrt (DLR), 51170 Köln, Germany*

²*Department of Physics, Heinrich-Heine Universität Düsseldorf, Universitätsstr. 1, 40225 Düsseldorf, Germany*

(Dated: November 8, 2018)

We present a mode-coupling theory (MCT) for the high-density dynamics of two-dimensional spherical active Brownian particles (ABP). The theory is based on the integration-through-transients (ITT) formalism and hence provides a starting point for the calculation of non-equilibrium averages in active-Brownian particle systems. The ABP are characterized by a self-propulsion velocity v_0 , and by their translational and rotational diffusion coefficients, D_t and D_r . The theory treats both the translational and the orientational degrees of freedom of ABP explicitly. This allows to study the effect of self-propulsion of both weak and strong persistence of the swimming direction, also at high densities where the persistence length $\ell_p = v_0/D_r$ is large compared to the typical interaction length scale. While the low-density dynamics of ABP is characterized by a single Péclet number, $Pe = v_0^2/D_r D_t$, close to the glass transition the dynamics is found to depend on Pe and ℓ_p separately. At fixed density, increasing the self-propulsion velocity causes structural relaxation to speed up, while decreasing the persistence length slows down the relaxation. The theory predicts a non-trivial idealized-glass-transition diagram in the three-dimensional parameter space of density, self-propulsion velocity and rotational diffusivity. The active-MCT glass is a nonergodic state where correlations of initial density fluctuations never fully decay, but also an infinite memory of initial orientational fluctuations is retained in the positions.

I. INTRODUCTION

The collective dynamics of self-propelled particles and the related behavior of dense suspensions of microswimmers have received an increasing amount of attention in the past few years. The physical principles of this dynamics are relevant for many biophysical questions. For example, mechanisms at work in wound healing (tissue repair) have been likened to the collective dynamics found in model microswimmer systems [1–5]. The collective dynamics of bacteria colonies [6], as well as the dynamics of the cell cytoskeleton show slow dynamics typically associated with that arising from crowding effects at high densities and associated glass-like slowing down [7–9].

Colloidal self-propelled particles provide paradigmatic model systems to study the qualitative effects of swimming, and more generically the generic features of a broad class of intrinsically non-equilibrium matter. In experiment, self-phoretic Brownian particles provide a good realization of this model. Half-capped “Janus particles” provide a surface-mediated mechanism to convert energy provided by light fields or chemical fuel into directed motion, superimposed on the Brownian translational and rotational diffusion of passive colloids [10–14].

One of the simplest theoretical models in this context is that of active Brownian particles (ABP) [15, 16]. These are orientable colloidal particles that undergo “passive” translational and rotational Brownian motion (ignoring hydrodynamic interactions in the following), and in addition an “active” drift along a body-fixed orientation axis due to intrinsic self-propulsion forces. In two spatial dimensions, particles are described by their positions \vec{r}_i and orientation angles θ_i with respect to a fixed direction in space. Here, $i = 1, \dots, N$ labels the particles. The equations of motion read, in the case of spherically

symmetric interaction forces,

$$d\vec{r}_i = \vec{F}_i/\zeta dt + \sqrt{2D_t} d\vec{W}_i + v_0 \vec{\sigma}(\theta_i) dt, \quad (1a)$$

$$d\theta_i = \sqrt{2D_r} dW_{\theta_i}, \quad (1b)$$

where $\vec{\sigma}(\theta) = (\cos \theta, \sin \theta)^T$ is the orientation vector. We will abbreviate $\vec{\sigma}_i = \vec{\sigma}(\theta_i)$. The elements of dW are independent Wiener processes, and the \vec{F}_i are the interaction forces. The friction coefficient $\zeta = 1/\beta D_t$ is taken to obey the fluctuation-dissipation theorem for the translational Brownian motion of the passive-particle system, with inverse temperature β . The key parameters characterizing the dynamics of a single spherical ABP are D_t , D_r , and v_0 : the translational short-time diffusion coefficient, the rotational diffusion coefficient, and the self-propulsion velocity. Although for a passive colloid, D_r and D_t are coupled due to the hydrodynamics of the solvent, for spherical ABP it makes sense to treat D_r as an independent model parameter. Different self-propulsion mechanisms may impose different persistence effects on the orientation, and to some extent these can be captured by varying D_r [17].

We focus on spherical ABP with strongly repulsive interactions, modeled by the equilibrium structure of a hard-sphere suspension. At high densities, such systems (with suitable size polydispersity) are known from simulation to form glasses [18–20], as do related active-particle models [5, 16, 21–25].

The theory of ABP has been extensively studied at low and moderate densities [26–30]. At large time scales, $D_r t \gg 1$, an “effective-diffusion limit” can be performed to map the dynamics of the dilute system onto Brownian motion with an effective diffusion coefficient: $D_{\text{eff}} = D_t + D_{\text{act}} = D_t(1 + Pe/2)$, where $Pe = v_0^2/D_r D_t$ defines the relevant Péclet number and $D_{\text{act}} = v_0^2/2D_r$ is an activity-

induced diffusivity. Accounting for this enhancement of diffusivity, many properties of dilute ABP suspensions and their phase behavior can be explained [26, 27]. The mapping however requires that all relevant length scales in the problem are large compared to the average swim length $\ell_p = v_0/D_r$, and that one probes the system on length scales larger than that [28, 29].

The high-density dynamics of ABP is less well explored. To describe glassy behavior of active systems, theories of the glass transition have been extended from the passive near-equilibrium case to include self propulsion [24, 31–36], using various different models and approximations. One particular reference point for the passive Brownian system is the mode-coupling theory of the glass transition (MCT), both in 3D [37] and in 2D [38]. MCT has been extended to deal with spherical ABP in the effective-diffusion limit [32]. In this limit, the equations of motion, Eq. (1), can be formally reduced to eliminate the orientation angles θ_i as explicit variables, in a procedure akin to the well-known reduction of the phase-space Langevin equation to the configuration-space Brownian dynamics. One obtains $d\vec{r}_i = \vec{F}_i/\zeta_{\text{eff}} + \sqrt{2D_t} d\vec{W}_i$ where ζ_{eff} is an effective friction coefficient. The resulting MCT takes the same form as the passive-equilibrium theory, with an activity-dependent prefactor in the memory kernel that reflects the non-equilibrium nature of the system through a violation of the fluctuation-dissipation theorem, $\zeta_{\text{eff}} \neq 1/\beta D_t$. Consequently, activity enters this theory only through the Péclet number Pe . This MCT approach extends easily to mixtures of active and passive particles [39]. It predicts a shift of the glass transition to higher densities, in qualitative agreement with simulation results.

However, the approach to a glass transition implies transient caging of particles on a length scale $\ell_c \sim 0.1\sigma$ (where σ is a typical particle size), over increasingly long times. It is not evident that the effective-diffusion approach remains valid as the condition $\ell_c < \ell_p$ is easily violated for typical swim speeds used in simulation and experiment. This calls for a theoretical treatment that starts directly from Eq. (1), rather than from a further reduced description of the dynamics.

Besides the ABP, the best studied model of active particles to date is the one proposed by Berthier, Szamel, and coworkers [24, 34], that of active Ornstein-Uhlenbeck particles (AOUP). Here, particles are described by their positions and an activity vector that represents the swimming direction and evolves according to an Ornstein-Uhlenbeck process providing colored noise for the evolution of the positions. The model thus belongs to a class where activity is modeled as leading to a persistent random walk of the particles [40–42]. This and related models have been studied in simulation [22, 23, 25, 43, 44] as the extension of paradigmatic passive glass formers to the non-equilibrium regime. A theoretical treatment based on MCT was established [34], under the simplifying assumption that the particle positions evolve on a time scale larger than the time scale governing the

evolution of the activity vector. This is not unlike the effective-diffusion approximation made in previous studies of high-density ABP systems. Predictions of the AOUP-MCT have been tested in computer simulation [44]. In the “athermal” case where activity is the sole driving force, the glass transition was found to depend non-monotonically on the activity strength [34]. This appears to be different for “thermal” ABP, according to present simulation results. Thus the connection among different models of active colloidal systems remains to be studied in more detail.

In this paper, we develop a MCT of spherical ABP that treats both the positional and orientational degrees of freedom on equal footing. This avoids the reduction to a near-equilibrium or an effective-diffusion description, and allows to study the qualitative effects of self-propulsion of various persistence lengths in the high-density regime. In particular it allows to study the limits $D_r \rightarrow 0$ and $D_r \rightarrow \infty$ as interesting reference cases [45] that provide valuable insight into the mechanisms by which swimming modifies the caging dynamics; Our approach is based on the integration-through transients (ITT) formalism as a formal approach to deal with the self-propulsion force as an arbitrarily strong perturbation of the passive-equilibrium dynamics.

The paper is organized as follows: in Sec. II we derive the MCT for two-dimensional spherical ABP, including rotational degrees of freedom. Section III shows numerical results for the dynamical density correlation functions close to the glass transition; Sec. IV is devoted to a discussion of the dependence of the glass-transition point on activity. Section V concludes.

II. MODE-COUPLING THEORY

The statistical information of the dynamics of a system composed of N spherical ABP is encoded in the Smoluchowski equation for the configuration-space distribution function $p(\Gamma, t)$, i.e., the probability density that corresponds to the Markov process described by the stochastic differential equations Eq. (1). Here $\Gamma = (\Gamma_r, \Gamma_\theta) = (\vec{r}_1, \dots, \vec{r}_N, \theta_1, \dots, \theta_N)$ labels points in configuration space. There holds $\partial_t p(\Gamma, t) = \Omega(\Gamma)p(\Gamma, t)$ with the Smoluchowski operator

$$\begin{aligned} \Omega &= \sum_{j=1}^N D_t \vec{\nabla}_j \cdot (\vec{\nabla}_j - \beta \vec{F}_j) + D_r \partial_{\theta_j}^2 - v_0 \vec{\nabla}_j \cdot \vec{o}(\theta_j) \\ &= \Omega_{\text{eq}}(D_t, D_r) + \delta\Omega(v_0), \end{aligned} \quad (2)$$

where $\delta\Omega(v_0) = -v_0 \sum_j \vec{\nabla}_j \cdot \vec{o}(\theta_j)$ is the term that represents the active motion. The interaction forces are assumed to follow from a spherically symmetric interaction potential, $\vec{F}_j = -\vec{\nabla}_j U(\Gamma_r)$.

Equation (2) for $v_0 = 0$ describes the passive Brownian system. It admits the equilibrium solution $p_{\text{eq}}(\Gamma_r) \propto \exp[-\beta U(\Gamma_r)]$. The integration-through transients (ITT)

formalism expresses averages of observables in the non-equilibrium system through history integrals involving transient correlation functions, i.e., correlation functions that contain the full non-equilibrium time evolution but are taken with the equilibrium distribution function. The starting point of ITT is the identity $\exp[\Omega t] = 1 + \int_0^t dt' \exp[\Omega t'] \Omega$. Using this identity to rewrite $p(t) = \exp[\Omega t] p(0)$, and assuming that for $t = 0$ the system starts in equilibrium, one gets a generalized Green-Kubo formula for any observable A . For the special case of the spherical ABP system,

$$\langle A \rangle_t = \langle A \rangle_{\text{eq}} - \beta v_0 \int_0^t dt' \left\langle \sum_{j=1}^N \vec{o}_j \cdot \vec{F}_j e^{\Omega^\dagger t' A} \right\rangle_{\text{eq}}. \quad (3)$$

The desire to evaluate expressions like this prompts the development of a theory of transient correlation functions. In the following, we will drop the subscript ‘‘eq’’ and implicitly perform all averages over the equilibrium distribution.

The collective motion of the particles is described by the local density fluctuations, $\varrho(\vec{r}, \theta) = \sum_{j=1}^N \delta(\vec{r} - \vec{r}_j) \delta(\theta - \theta_j)$, respectively their Fourier transform

$$\delta \varrho_l(\vec{q}) = \sum_{j=1}^N e^{i\vec{q} \cdot \vec{r}_j} e^{il\theta_j} / \sqrt{N}. \quad (4)$$

with integer angular indices $l = -\infty, \dots, \infty$. We assume the system to remain in a homogeneous, translationally invariant and isotropic state. Then, the equilibrium static structure factor matrix depends on the wave vector only through $q = |\vec{q}|$,

$$S_{ll'}(q) = \langle \delta \varrho_l^*(\vec{q}) \delta \varrho_{l'}(\vec{q}) \rangle. \quad (5)$$

Also the two-point density correlation functions are diagonal in wave-vector space under these conditions. Since the interaction potential is spherically symmetric, the matrix $\mathbf{S}(q)$ takes the simple form

$$S_{ll'}(q) = \delta_{ll'} (1 + \delta_{l0} (S_q - 1)), \quad (6)$$

i.e., it is the unit matrix with its (00) element replaced by S_q , the usual static structure factor of the equilibrium system of spherical particles.

The time-dependent transient density correlation functions are defined as

$$S_{ll'}(\vec{q}, t) = \left\langle \delta \varrho_l^*(\vec{q}) e^{\Omega^\dagger t} \delta \varrho_{l'}(\vec{q}) \right\rangle. \quad (7)$$

Here, the adjoint (or backward) Smoluchowski operator provides the temporal evolution,

$$\Omega^\dagger = \sum_{j=1}^N D_t \left(\vec{\nabla}_j + \beta \vec{F}_j \right) \cdot \vec{\nabla}_j + D_r \partial_{\theta_j}^2 + v_0 \vec{o}_j \cdot \vec{\nabla}_j. \quad (8)$$

We use the convention that this operator acts to everything on its right, but not on the distribution function

itself. There holds $\mathbf{S}(\vec{q}, 0) = \mathbf{S}(q)$. The normalized correlator is defined by $\Phi(\vec{q}, t) = \mathbf{S}(\vec{q}, t) \cdot \mathbf{S}^{-1}(q)$.

The correlation functions are defined in a specific laboratory frame of reference, with respect to which particle orientations are measured. For this reason, the correlation functions depend a priori on the direction of the wave vector \vec{q} . However, there hold simple transformation rules to transform the correlators to a rotated reference frame. Consider a rotation around an angle α , $\vec{r} \mapsto \vec{r}' = \mathbf{D}(\alpha) \cdot \vec{r}$ and $\theta \mapsto \theta' = \theta + \alpha$, with $\mathbf{D} \cdot \mathbf{D}^T = 1$ a rotation matrix. This changes $\delta \varrho_l(\vec{q}) \mapsto \delta \varrho_l(\vec{q}') \exp[i l \alpha]$ where $\vec{q}' = \mathbf{D} \cdot \vec{q}$. The transformation is thus given by a unitary representation $\mathbf{u}(\alpha)$ of the orientation group $SO(1)$, given by $u_{ll'} = \exp[-il\alpha] \delta_{ll'}$. (There holds $\mathbf{u}(\alpha) \cdot \mathbf{u}(\beta) = \mathbf{u}(\alpha + \beta)$, $\mathbf{u}(\alpha) \mathbf{u}^\dagger(\alpha) = \mathbf{1}$, $\mathbf{u}(0) = \mathbf{1}$, and $\mathbf{u}(\alpha + 2\pi) = \mathbf{u}(\alpha)$, as well as $\det \mathbf{u} = 1$.) One easily shows that the Smoluchowski operator itself is invariant under rotation, $\Omega(\Gamma) = \Omega'(\Gamma')$, separately in all its terms. (To see this, recall $\vec{\partial}' \cdot \vec{o}(\theta') = (\mathbf{D}^{-1} \cdot \vec{\partial}) \cdot \vec{o}(\theta + \alpha) = \vec{\partial} \cdot \mathbf{D} \cdot \vec{o}(\theta + \alpha) = \vec{\partial} \cdot \vec{o}(\theta)$). Under rotation, the equilibrium distribution function remains invariant, and thus one obtains the transformation rule

$$\mathbf{S}(\vec{q}, t) \mapsto \mathbf{u}(\alpha) \cdot \mathbf{S}(\vec{q}', t) \cdot \mathbf{u}^\dagger(\alpha). \quad (9)$$

We will make use of this relation to restrict the discussion of the correlation functions to wave vectors aligned with a particular spatial direction, chosen by $\vec{q} = q \vec{e}_y$. Note that Eq. (9) confirms that $S_{00}(q, t)$ is in fact invariant under rotations.

An equation of motion for $\mathbf{S}(\vec{q}, t)$ can be derived using the Mori-Zwanzig projection operator formalism. Introduce the projection operator onto density fluctuations,

$$\mathcal{P} = \sum_{l_1 l_2} \delta \varrho_{l_1}(\vec{q}) S_{l_1 l_2}^{-1}(q) \langle \delta \varrho_{l_2}^*(\vec{q}) \rangle, \quad (10)$$

and set $\mathcal{Q} = 1 - \mathcal{P}$. One now writes $\partial_t \exp[\Omega^\dagger t] = \Omega^\dagger (\mathcal{P} + \mathcal{Q}) \exp[\Omega^\dagger t]$ and rewrites the second term using the Dyson decomposition

$$e^{\Omega^\dagger t} = e^{\Omega^\dagger \mathcal{Q} t} + \int_0^t dt' e^{\Omega^\dagger \mathcal{Q}(t-t')} \Omega^\dagger \mathcal{P} e^{\Omega^\dagger t'} \quad (11)$$

to obtain

$$\begin{aligned} \partial_t \mathbf{S}(\vec{q}, t) &= -\boldsymbol{\omega}(\vec{q}) \cdot \mathbf{S}^{-1}(q) \cdot \mathbf{S}(\vec{q}, t) \\ &+ \int_0^t dt' \mathbf{K}(\vec{q}, t - t') \cdot \mathbf{S}^{-1}(q) \cdot \mathbf{S}(\vec{q}, t') \end{aligned} \quad (12)$$

where $\boldsymbol{\omega}(\vec{q})$ generalizes the collective diffusion matrix,

$$\begin{aligned} \omega_{ll'}(\vec{q}) &= - \left\langle \delta \varrho_l^*(\vec{q}) \Omega^\dagger \delta \varrho_{l'}(\vec{q}) \right\rangle \\ &= (q^2 D_t + l^2 D_r) \delta_{ll'} - \frac{i q v_0}{2} e^{-i(l-l')\vartheta_q} S_{ll'}(q) \delta_{|l-l'|, 1}, \end{aligned} \quad (13)$$

writing $\vec{q} = q(\cos \vartheta_q, \sin \vartheta_q)^T$. The memory kernel $\mathbf{K}(\vec{q}, t)$ is given by

$$K_{ll'}(\vec{q}, t) = \left\langle \delta \varrho_l^*(\vec{q}) \Omega^\dagger \mathcal{Q} e^{\mathcal{Q} \Omega^\dagger \mathcal{Q} t} \mathcal{Q} \Omega^\dagger \delta \varrho_{l'}(\vec{q}) \right\rangle \quad (14)$$

It describes the renormalization of the diffusion matrix due to many-body interactions.

For small density, $\rho = N/V \rightarrow 0$ (where V is the system volume), one can drop the memory kernel in Eq. (12). The formal solution, $\mathbf{S}(\vec{q}, t) = \exp[-\boldsymbol{\omega}(\vec{q})t]$, reproduces the exact solution as discussed in 3D [30].

The slowing down of the dynamics close to a glass transition is driven by slow positional density fluctuations. This suggests to split the time-evolution operator, $\Omega = \Omega_T(D_t, v_0) + \Omega_R(D_r)$. The matrix elements of the translational and rotational parts will be written as $\boldsymbol{\omega}(\vec{q}) = \boldsymbol{\omega}_T(\vec{q}) + \boldsymbol{\omega}_R(\vec{q})$, i.e., $\omega_{R, ll'}(\vec{q}) = l^2 D_r \delta_{ll'}$. Correspondingly, we decompose the memory kernel into four contributions, $\mathbf{K}(t) = \mathbf{K}^{TT}(t) + \mathbf{K}^{TR}(t) + \mathbf{K}^{RT}(t) + \mathbf{K}^{RR}(t)$, given by replacing the operators Ω^\dagger appearing to the right and to the left of the reduced propagator in Eq. (14) by their decompositions.

Since in our model of spherical ABP, the rotational degrees of freedom never slow down, all contributions to the memory kernel involving Ω_R^\dagger vanish, and there holds $\mathbf{K}(t) = \mathbf{K}^{TT}(t)$. (This is also explicitly checked in a mode-coupling approximation.)

To describe slow dynamics arising from a coupling of translational modes, we follow the standard procedure of MCT and rewrite the diffusion kernel $\mathbf{K}^{TT}(t)$ in terms of a friction kernel. To do so, introduce a further projector,

$$\mathcal{P}' = - \sum_{l_1 l_2} \delta \varrho_{l_1}(\vec{q}) \psi_{l_1 l_2}(\vec{q}) \langle \delta \varrho_{l_2}^*(\vec{q}) \Omega_T^\dagger \rangle \quad (15)$$

where $\psi(\vec{q}) = \boldsymbol{\omega}_T^{-1}(\vec{q})$ normalizes the projector. We now decompose the propagator that appears in Eq. (14) according to

$$e^{\mathcal{Q} \Omega_T^\dagger \mathcal{Q} t} = e^{\mathcal{Q} \Omega_T^\dagger \mathcal{Q}' \mathcal{Q} t} + \int_0^t dt' e^{\mathcal{Q} \Omega_T^\dagger \mathcal{Q}'(t-t')} \mathcal{Q} \Omega_T^\dagger \mathcal{P}' \mathcal{Q} e^{\mathcal{Q} \Omega_T^\dagger \mathcal{Q}' \mathcal{Q} t'}. \quad (16)$$

This results in

$$\mathbf{K}^{TT}(\vec{q}, t) = \mathbf{M}(\vec{q}, t) - \int_0^t \mathbf{K}^{TT}(\vec{q}, t-t') \cdot \boldsymbol{\omega}_T^{-1}(\vec{q}) \cdot \mathbf{M}(\vec{q}, t') \quad (17)$$

where we have defined the friction memory kernel

$$M_{ll'}(\vec{q}, t) = \left\langle \delta \varrho_l^*(\vec{q}) \Omega_T^\dagger \mathcal{Q} e^{\mathcal{Q} \Omega_T^\dagger \mathcal{Q}' \mathcal{Q} t} \mathcal{Q} \Omega_T^\dagger \delta \varrho_{l'}(\vec{q}) \right\rangle. \quad (18)$$

Note that $\mathbf{M}(\vec{q}, t)$ and $\mathbf{K}^{TT}(\vec{q}, t)$ only differ in their time evolution. In the context of passive Brownian particles, the operator appearing in Eq. (18) is also referred to as the one-particle irreducible Smoluchowski operator.

Equations (12) and (17) can be combined to a time-evolution equation for the density correlation functions

that is a suitable starting point for approximations of the slow dynamics arising from the slow evolution of positional density fluctuations,

$$\begin{aligned} & \boldsymbol{\omega}_T^{-1}(\vec{q}) \cdot \partial_t \mathbf{S}(\vec{q}, t) + [\mathbf{S}^{-1}(q) + \boldsymbol{\omega}_T^{-1}(\vec{q}) \cdot \boldsymbol{\omega}_R] \cdot \mathbf{S}(\vec{q}, t) \\ & + \int_0^t dt' \mathbf{m}(\vec{q}, t-t') \cdot (\partial_{t'} \mathbf{S}(\vec{q}, t') + \boldsymbol{\omega}_R \cdot \mathbf{S}(\vec{q}, t')) = \mathbf{0} \end{aligned} \quad (19a)$$

Here we have used that $\boldsymbol{\omega}_R \cdot \mathbf{S}^{-1}(q) = \boldsymbol{\omega}_R$ for the spherical ABP system we consider, and abbreviated

$$\mathbf{m}(\vec{q}, t) = \boldsymbol{\omega}_T^{-1}(\vec{q}) \cdot \mathbf{M}(\vec{q}, t) \cdot \boldsymbol{\omega}_T^{-1}(\vec{q}). \quad (19b)$$

Equations (19) are the starting point of mode-coupling approximations for glassy dynamics. Setting $v_0 = 0$, the matrices all become diagonal (since Ω_T^\dagger does not mix translational and rotational degrees of freedom in this case), and one recovers for $S_{00}(q, t)$ the standard Mori-Zwanzig equation used to derive MCT for Brownian spherical particles.

Rotational diffusion appears in Eqs. (19) in the form of a ‘‘hopping term’’ in the MCT language, viz. the last term under the integral in Eq. (19a). The original MCT only contains a convolution of the memory kernel with the time derivative of the density correlation function, viz. the first term under the integral in Eq. (19a). In this form the equations allow for an ideal glass transition: there exist solutions with a non-zero long-time limit $\lim_{t \rightarrow \infty} \mathbf{S}(\vec{q}, t) = \mathbf{F}(\vec{q}) \neq \mathbf{0}$. The presence of the density correlator itself in the convolution integral for $l \neq 0$ causes the corresponding solutions to ultimately decay exponentially: since rotation remains unhindered even in the dense system, the associated density fluctuations will decay on a time scale $1/(l^2 D_r)$. Note that Eq. (19) still allows for an ideal glass transition for all transient density correlation functions $S_{ll'}(\vec{q}, t)$ with $l = 0$.

The MCT approximation now consists of two intertwined steps: first the fluctuating forces $\mathcal{Q} \Omega_T^\dagger \delta \varrho_l(\vec{q})$ that appear in $\mathbf{M}(\vec{q}, t)$ are replaced by their overlap with density-fluctuation pairs. Using the short-hand notation $\delta \varrho_1 \equiv \delta \varrho_{l_1}(\vec{q}_1)$, one introduces the pair-density projector

$$\mathcal{P}_2 = \sum_{1,2,1',2'} \delta \varrho_1 \delta \varrho_2 \chi_{121'2'} \langle \delta \varrho_{1'}^* \delta \varrho_{2'}^* \rangle \quad (20)$$

with a suitable normalization matrix χ . Second, the resulting dynamical four-point correlation functions that involve the reduced dynamics are replaced by the product of two-point correlation functions propagated by the full dynamics,

$$\begin{aligned} & \langle \delta \varrho_{1'}^* \delta \varrho_{2'}^* e^{\mathcal{Q} \Omega_T^\dagger \mathcal{Q}' \mathcal{Q} t} \delta \varrho_{l_1} \delta \varrho_{l_2} \rangle \\ & \approx \langle \delta \varrho_{1'}^* e^{\Omega^\dagger t} \delta \varrho_{l_1} \rangle \langle \delta \varrho_{2'}^* e^{\Omega^\dagger t} \delta \varrho_{l_2} \rangle + \{1' \leftrightarrow 2'\} \end{aligned} \quad (21)$$

together with a consistent approximation of χ . For a detailed derivation of the MCT expression for the memory

kernel, we refer to Appendix A. One gets

$$m_{ll'}(\vec{q}, t) = \frac{\rho^2}{2N} \sum_{\vec{k}+\vec{p}=\vec{q}} \sum_{l_1 l_2 l'_1 l'_2} \mathcal{V}_{ll_1 l_2}^\dagger(\vec{q}, \vec{k}, \vec{p}) \times S_{l_1 l'_1}(\vec{k}, t) S_{l_2 l'_2}(\vec{p}, t) \mathcal{V}_{l'_1 l'_2}(\vec{q}, \vec{k}, \vec{p}) \quad (22)$$

The vertices are given by $\mathcal{V}_{ll_1 l_2}^\dagger(\vec{q}, \vec{k}, \vec{p}) = \sum_m (\omega_T^{-1}(\vec{q}))_{lm} \mathcal{W}_{ml_1 l_2}^\dagger(\vec{q}, \vec{k}, \vec{p})$ and $\mathcal{V}_{ll_1 l_2}(\vec{q}, \vec{k}, \vec{p}) = \sum_m (\omega_T^{-1})_{lm}(\vec{q}) \mathcal{W}_{ml_1 l_2}(\vec{q}, \vec{k}, \vec{p})$, with

$$\begin{aligned} \mathcal{W}_{ll_1 l_2}^\dagger(\vec{q}, \vec{k}, \vec{p}) &= D_t \delta_{l, l_1 + l_2} \left(\vec{q} \cdot \vec{k} c_{l_1 l_1}(k) + \vec{q} \cdot \vec{p} c_{l_2 l_2}(p) \right) \\ &+ \frac{i v_0}{2\rho} \delta_{|l-l_1-l_2|, 1} S_{l_1 l_1}(q) \left(k e^{-i(l-l_1-l_2)\theta_k} \tilde{S}_{l-l_2, l_1}(k) \right. \\ &\left. + p e^{-i(l-l_1-l_2)\theta_p} \tilde{S}_{l-l_1, l_2}(p) - q e^{-i(l-l_1-l_2)\theta_q} \right) \quad (23) \end{aligned}$$

where we have defined $\tilde{S}_{ll}(k) = S_{l'l'}^{-1}(k) S_{ll}(k)$. The left vertex is the same as in equilibrium,

$$\mathcal{W}_{ll_1 l_2}(\vec{q}, \vec{k}, \vec{p}) = D_t \delta_{l, l_1 + l_2} \left(\vec{q} \cdot \vec{k} c_{l_1 l_1}(k) + \vec{q} \cdot \vec{p} c_{l_2 l_2}(p) \right) \quad (24)$$

It differs from \mathcal{W}^\dagger because the time-evolution operator Ω^\dagger is not self-adjoint with respect to the scalar product defined by the equilibrium averages.

For $v_0 = 0$, these equations reduce to the equilibrium MCT expressions. In particular, in this case \mathcal{V} and \mathcal{V}^\dagger do no longer explicitly depend on D_t . In the active case, $v_0 \neq 0$, one readily checks that the explicit dependence on D_t still cancels in the memory kernel if the self-propulsion velocity is expressed in terms of a Péclet number $Pe_t = v_0 \sigma / D_t$, where σ is a typical particle diameter. There is no dependence on D_r in the memory kernel, and therefore the Péclet number $Pe = v_0^2 / D_t D_r$ does not assume the natural role in determining the MCT dynamics that it has for the low-density system.

The MCT approximation preserves the transformation properties of the correlation functions under rotation, Eq. (9). In fact, the same transformation law is required for all the quantities that appear in the Mori-Zwanzig equations, Eq. (12) or (19a). In particular, $\omega(\vec{q}) \mapsto \mathbf{u}(\alpha) \cdot \omega(\vec{q}') \cdot \omega^\dagger(\alpha)$ is easily checked. For the MCT vertices, a straightforward calculation shows $\mathcal{W}_{ll_1 l_2}^\dagger(\vec{q}, \vec{k}, \vec{p}) \mapsto \mathcal{W}_{l'l'_1 l'_2}^\dagger(\vec{q}', \vec{k}', \vec{p}') u_{ll'}(\alpha) u_{l'_1 l_1}^\dagger(\alpha) u_{l'_2 l_2}^\dagger(\alpha)$ and equivalently for $\mathcal{W}_{ll_1 l_2}(\vec{q}, \vec{k}, \vec{p})$, i.e., all terms that appear in the MCT expression for $\mathbf{m}(\vec{q}, t)$ transform like tensors.

The fact that the MCT approximation preserves the transformation properties of the correlation functions under rotation, allows us to pick a coordinate system where \vec{q} is aligned along a coordinate axis, $\vec{q} = q \vec{e}_y$, say. By using the unitary transformation property, all correlation functions entering the MCT memory kernel can be rewritten in terms of those evaluated with \vec{q} aligned along the same axis. For completeness, this form of the MCT equations is documented in Appendix B. This allows to

reduce the numerical calculation to wave vectors along a single spatial axis.

The MCT equations have been solved numerically on a grid of 128 wave numbers equally spaced up to $|\vec{q}| \leq Q$ with $Q\sigma = 50$. For the angular indices, a cutoff $|l| \leq L$ with $L = 1$ has been introduced. Some results have been checked with $L = 2$, but the effects were minor. The presence of the ‘‘hopping’’ term with its singular structure (imposed by $\omega_{R,00} = 0$) poses a numerical problem at long times. We have developed an extension of the standard algorithm that is usually employed to solve MCT equations, and that we outline in Appendix C.

To determine the MCT vertex, the equilibrium static structure factor is needed. In odd dimensions, the Percus-Yevick approximation provides a reasonably accurate analytical expression. However, in even dimensions, no such analytical solution is known. We use the Baus-Colot expression for $S(q)$ that is known to be close to simulation data.

We fix units of length and time by the particle diameter $\sigma = 1$ and the translational free-diffusion time $\sigma^2 / D_t = 1$. Densities are reported as packing fractions, $\phi = (\pi/4)\rho\sigma^2$. With the chosen parameters, we obtain a glass transition in the passive hard-disk system at a critical packing fraction $\phi_c \approx 0.7207$; this is in reasonable agreement with the value reported in earlier work [38]. In comparison to this work, we have improved the numerical evaluation of the wave-vector integrals appearing in the MCT memory kernel; see Appendix B for details.

III. DYNAMICS

Exemplary MCT results for the density correlation functions $\Phi_{00}(\vec{q}, t)$ are shown in Fig. 1. A wave number $q\sigma = 8$ in the vicinity of the main peak of the equilibrium $S(q)$ was chosen. The density correlation functions show the qualitative features expected for dense colloidal suspensions nearing dynamical arrest: after an initial relaxation, a plateau emerges at high densities that extends over an increasingly large intermediate-time window as the density is increased. The final relaxation from this plateau to zero is termed structural relaxation, and its characteristic time increases strongly with increasing density. At the highest densities shown, structural relaxation becomes ineffective and is not seen over the full time window accessible to the numerical solution scheme. Hence, $\lim_{t \rightarrow \infty} \Phi_{00}(\vec{q}, t) = F_{00}(\vec{q}) > 0$. This non-zero positive non-ergodicity parameter signals the appearance of an ideal glass.

With increasing self-propulsion velocity v_0 , the dynamics speeds up, as shown in the upper panel of the figure. This is qualitatively expected, since self-propulsion renders the particle motion more vivid, and this opposes the slow dynamics. This result is also qualitatively consistent with earlier Brownian-dynamics (BD) simulation studies of three-dimensional ABP [18]. (Note that there, stationary-state non-equilibrium correlation func-

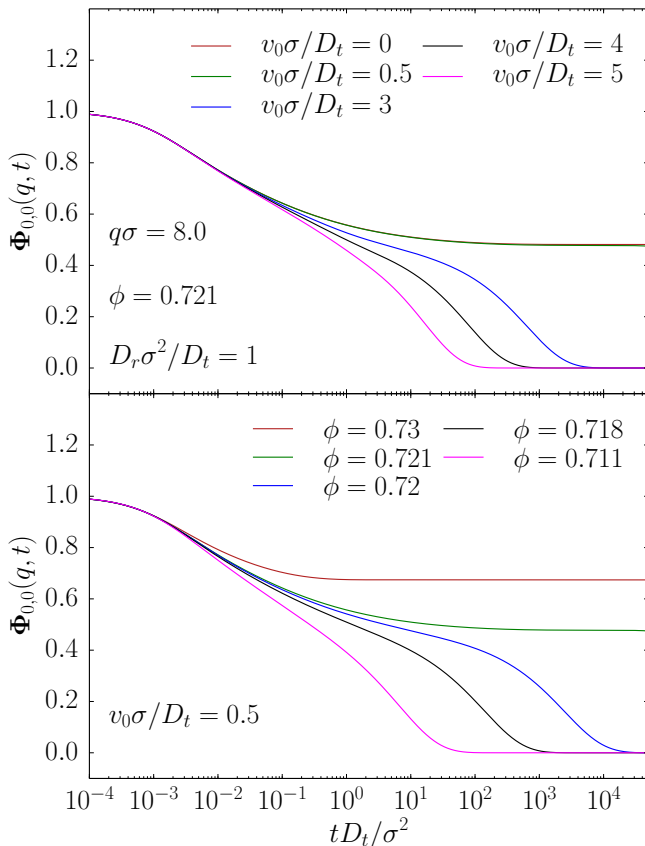


FIG. 1. Transient density correlation functions $\Phi_{00}(q, t)$ of a hard-disk ABP system within MCT, at wave number $q\sigma = 8$ and for $D_r = 1$. Upper panel: functions at constant packing fraction $\phi = 0.721$ above the passive glass transition, for increasing v_0 (right to left) as labeled. Lower panel: functions at constant self-propulsion velocity v_0 , for increasing packing fraction (left to right).

tions were reported, while the central object of our MCT are the transient non-equilibrium, equilibrium-averaged correlation functions.)

For small enough self-propulsion velocity, the glass remains stable at sufficiently high density. This is exemplified by the lower panel of Fig. 1, where curves for constant $v_0 = 0.5 D_t/\sigma$ are shown. At the highest packing fractions shown, no sign of structural relaxation is seen in the numerical results over the time window covered in the figure.

Hence, for small enough but finite v_0 MCT predicts an ideal “active glass”. As the lower panel of Fig. 1 demonstrates, the signature of the transition to this active glass is qualitatively as for the passive ideal glass: with increasing density at fixed v_0 , structural relaxation dramatically slows down until it completely arrests at the transition density ϕ_c . Further increasing the density causes the nonergodicity parameter to increase. The ideal glass transition is discontinuous in the sense that the long-time limit of the density correlation functions jumps from zero in the liquid ($\phi < \phi_c$) to a finite value

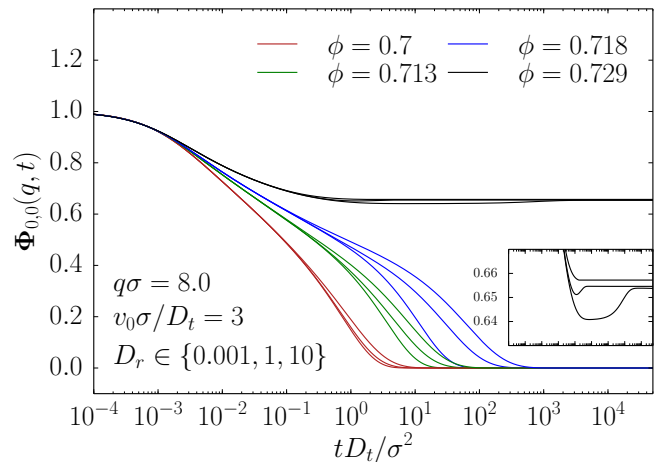


FIG. 2. Density correlation functions $\Phi_{00}(\vec{q}, t)$ for packing fractions $\phi = 0.7, 0.713, 0.718,$ and 0.729 (groups of lines from left to right) and self-propulsion velocity $v_0 = 3 D_t/\sigma$, for different values of the rotational diffusion coefficient, $D_r = 1/1000, 1,$ and 10 (left to right). The inset provides a zoom of the $\phi = 0.729$ curves.

at ϕ_c .

These results suggest that there is a line of ideal glass transitions (ϕ_c, v_0^c) in the density–self-propulsion plane. This line shifts to increasing density with increasing v_0 . Qualitatively, this result has been derived in earlier extensions of MCT that do not account for orientational degrees of freedom explicitly [32].

With the present approach, the influence of the rotational diffusion coefficient on the dynamics can be studied. Figure 2 exemplifies the effects of increasing D_r on the dynamics at fixed self-propulsion velocity. Keeping the other parameters fixed, an increase in D_r leads to a slowing down of the structural-relaxation dynamics. Qualitatively, this is expected from the argument that faster reorientation of the individual particles causes the self-propulsion to be less effective in melting nearest neighbor cages, since for the latter process a certain persistence of the self-propulsion force in a specific direction needs to be maintained. The slowing down with increasing D_r is more pronounced at higher densities: while at $\phi = 0.7$, the final relaxation of the curves shown in Fig. 2 spreads out by about a factor 2, the same change in D_r causes the structural-relaxation time to change by a factor of about 10 at $\phi = 0.718$.

The structural relaxation dynamics of the weakly active system shows the same qualitative features as they are known from the passive system. In particular, the structural relaxation process can be well described by a stretched-exponential function in time for the cases shown in Figs. 1 and 2. It is known from the passive system, that density fluctuations with wavelengths comparable to the particle size govern the slow dynamics.

For the active system, the persistence of self-propulsion sets another length scale, $\ell_p = v_0/D_r$. This suggests to

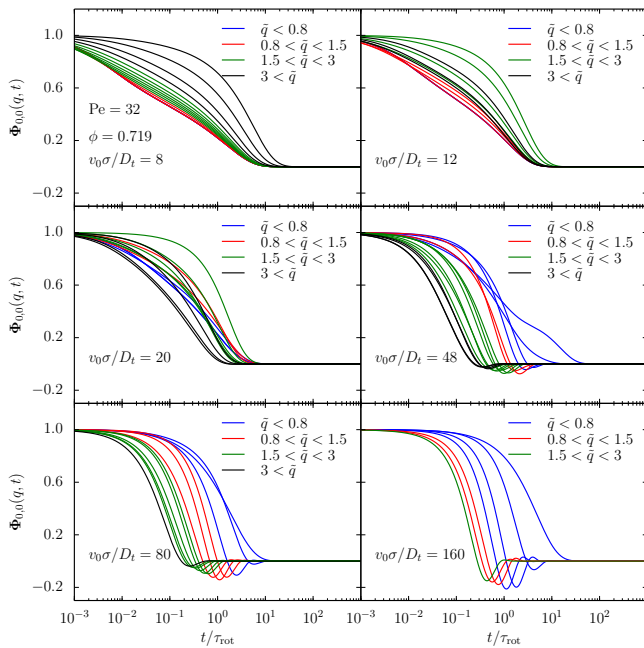


FIG. 3. Wave-number dependence of the transient density correlation functions $\Phi_{00}(q, t)$ for packing fraction $\varphi = 0.719$ just below the passive-glass transition, for different velocities as labeled, keeping the Péclet number $Pe = v_0^2/D_r D_t = 32$ fixed. From top left to bottom right, the values are $(v_0, D_r) = (8, 2)$, $(12, 4.5)$, $(20, 12.5)$, $(48, 64)$, $(80, 200)$, and $(160, 800)$. Wave numbers $\tilde{q} = q\ell_p/(2\pi)$ are given in units of the persistence length, $\ell_p = v_0/D_r$, and increase from right to left (in the top part of the curves). The panels correspond to $\ell_p = 4, 2.67, 1.6, 0.75, 0.4$, and 0.2 . Correlators are shown as functions of rescaled time, t/τ_{rot} , with the time scale set by the reorientational diffusion, $\tau_r = \sigma/D_r$.

discuss the effect of density fluctuations on length scales much larger, comparable to, and much smaller than the persistence length. Let us introduce a rescaled wave number $\tilde{q} = q\ell_p/(2\pi)$. The low-density dynamics of ABP exhibits three distinct regimes [30]: for $\tilde{q} \ll 1$ probe the dynamics on length scales large compared to ℓ_p , and hence see diffusive relaxation with a diffusion coefficient D_{eff} . For small length scales, probed by $\tilde{q} \gg 1$, the initial Brownian passive diffusion of the ABP is seen, and the density correlators decay diffusively, with diffusion coefficient D_t . Activity causes an intermediate regime $\tilde{q} \approx 1$ to appear, where the persistent swimming motion affects the relaxation of density fluctuations. Over the length scales probed in this regime, particles swim in a fixed direction and cause density fluctuations to decay in a damped-oscillatory fashion, leading to pronounced “undershoots” in the final relaxation.

The influence of high-density interactions on this single-particle picture is examined in Fig. 3. Here, state points close to the glass transition were chosen and to make connection to the low-density theory, different activities along a cut with constant Péclet number, $Pe = 32$, are shown. The panels of Fig. 3 correspond to in-

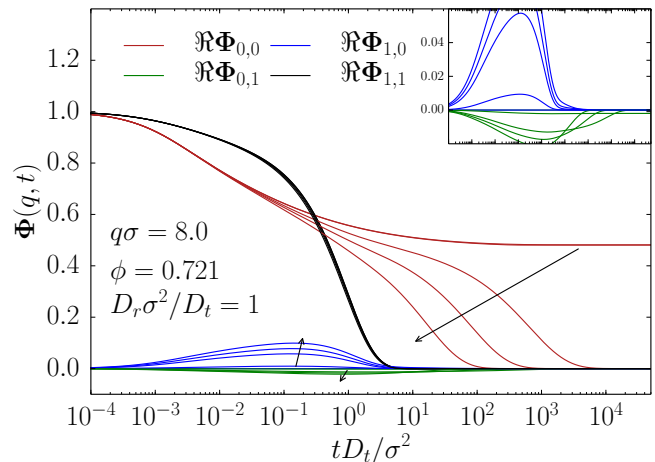


FIG. 4. Matrix elements of the transient density correlation matrix $\Phi(\vec{q}, t)$ at fixed packing fraction ϕ and rotational diffusion D_r , for increasing v_0 (right to left). The inset provides a zoom for the off-diagonal components.

creasing self-propulsion velocity (from top left to bottom right), and at fixed Pe , these correspond to decreasing persistence lengths. Essentially, the low-density scenario is recovered for the case $\ell_p < \sigma$, i.e., for large self-propulsion velocity. There, structural arrest is effectively destroyed by active driving, and the correlation functions decay on a time scale $\tau_{\text{rot}} = 1/D_r$, showing oscillations around $\tilde{q} \approx 1$ (cf. lower panels of Fig. 3).

For large persistence length, $\ell_p \gg \sigma$, the top panels of Fig. 3 demonstrate that the low-density scenario is absent. Here, all correlation functions decay without oscillations. This result can be interpreted as showing that once the interparticle length scale becomes smaller than ℓ_p , density fluctuations can no longer be translated by persistent motion; they relax by the combination of diffusion and activity-modified structural interactions. Coincidentally, for the $\ell_p \gg \sigma$ cases shown in Fig. 3, the intermediate-time plateau of structural relaxation begins to emerge at large \tilde{q} (corresponding to intermediate $q\sigma$).

The appearance of oscillatory relaxation in the density correlation functions of a Brownian system is a clear signature of non-equilibrium dynamics. Recall that the equilibrium Smoluchowski operator Ω_{eq} is negative semi-definite, i.e., it has non-positive real eigenvalues only. As a result, the corresponding auto-correlation functions are completely monotone functions: they can be written as superpositions of purely relaxing exponential functions with positive weights. This is a feature that is preserved under the MCT approximation.

To highlight the dynamics of the reorientational degrees of freedom, we show in Fig. 4 the matrix elements of $\Phi_{ll'}(\vec{q}, t)$ for $|l| \leq 1$. Only positive l, l' are shown for simplicity, and the case $l = l' = 0$ is repeated from above for reference. The $(ll') = (11)$ correlator reflects the decay of orientational order. It decays on the time scale $\tau_{\text{rot}} = \sigma/D_r$, with a final exponential re-

laxation. This is expected since in the spherical ABP model, rotation is not influenced by the packing of particles. Note that the decay of $\Phi_{11}(\vec{q}, t)$ is not purely exponential; even at low densities and without self propulsion, $\Phi_{11}(\vec{q}, t) \sim \exp[-q^2 D_t t] \exp[-D_r t]$. In general, the $(ll') = (11)$ correlator inherits a signature of the translational motion for $t \ll \tau_{\text{rot}}$, which is cut off by an exponential decay at $t \sim \tau_{\text{rot}}$.

The off-diagonal elements $(ll') = (01)$ and (10) of the transient density correlation function behave different from each other. In equilibrium, one expects the matrix of correlation functions to be symmetric (as is the case for example in the MCT developed for Newtonian non-spherical particles [46–48]). This symmetry is lost in the present theory because the time-evolution operator is not self-adjoint with respect to the equilibrium-weighted scalar product.

The off-diagonal elements vanish with $v_0 \rightarrow 0$, as expected from the structure of the Smoluchowski equation for spherical ABP. Interestingly, the correlation function $\Phi_{01}(\vec{q}, t)$ shows non-trivial slow dynamics that is coupled to the slow dynamics of the positional-density correlator $\Phi_{00}(\vec{q}, t)$. In particular it displays structural relaxation that slows down beyond the time scale τ_r over which orientational order decays. The correlation function $\Phi_{10}(\vec{q}, t)$ instead decays on the reorientational time scale τ_{rot} .

This observation can be rationalized by the peculiar structure of the equations of motion of spherical ABP: orientations influence the slow dynamics of the positions, but not vice versa. Thus, the evolution of positional density fluctuations, $\exp[\Omega^\dagger t] \delta \rho_0(\vec{q})$, will not be detectable in the subspace spanned by the orientations, $\delta \rho_1^*(\vec{q})$, for times $t \gg \tau_{\text{rot}}$. On the other hand, the impact of the time-evolved initial polar order, $\exp[\Omega^\dagger t] \delta \rho_1(\vec{q})$, on the positional density fluctuations of the system, $\delta \rho_0^*(\vec{q})$, persists until the time of overall structural relaxation, hence $S_{01}(\vec{q}, t) = \langle \delta \rho_0^*(\vec{q}) \exp[\Omega^\dagger t] \delta \rho_1(\vec{q}) \rangle$ decays as slow as $S_{00}(\vec{q}, t)$.

The usual quantification of the slow dynamics is in terms of the structural relaxation time τ . Following the operational definition used in many studies of glassy dynamics, we define τ as the time where the density-correlation function has decayed to 1% of its initial value, $\Phi_{00}(\vec{q}, \tau) = 0.01$.

Results for $\tau(\varphi)$ for a fixed self-propulsion velocity are shown in Fig. 5. As anticipated from the discussion above, the structural relaxation time strongly increases with increasing packing fraction, in a power-law fashion that is the hallmark of the approach to the MCT glass transition. At fixed v_0 , increasing D_r increases the structural relaxation time. For $D_r \rightarrow \infty$, the τ -vs- φ curve corresponding to the passive system is approached.

The data shown in Fig. 5 agree qualitatively with corresponding 3D results from BD simulations [18]. Again, similar results have been discussed for the AOUP system [44] and glassy tissue models [5], demonstrating that the MCT power law that describes the increase in relaxation

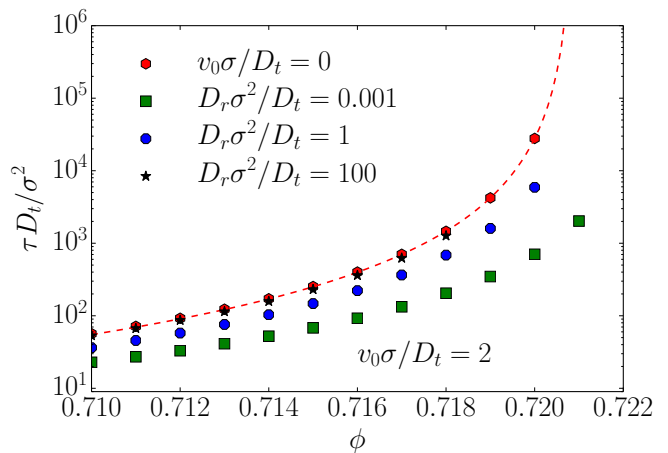


FIG. 5. Structural relaxation times $\tau(\phi, v_0, D_r)$ as a function of ϕ for fixed v_0 and different D_r (as indicated by the different symbols). Hexagon symbols connected by a dashed line correspond to the passive system.

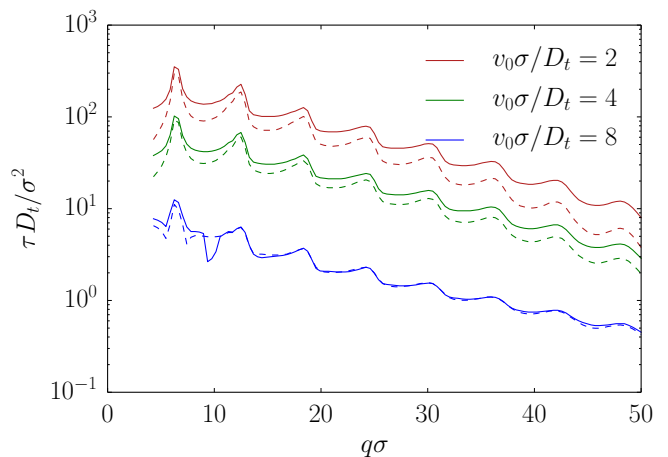


FIG. 6. Structural relaxation times $\tau(\phi, v_0, D_r)$ as a function of wavenumber q for fixed $D_r = 1 D_t / \sigma^2$ and various v_0 as indicated (increasing v_0 from top to bottom). Solid lines are extracted from the positional-density correlator $\Phi_{00}(\vec{q}, t)$, dashed lines from the orientational correlator $\Phi_{01}(\vec{q}, t)$.

time is quite robust.

The structural relaxation time depends on the wave number of the density fluctuations. The q -dependence of τ is shown for a fixed density and various self-propulsion velocities in Fig. 6. Both the slow relaxation times for $(ll') = (00)$ and (01) are shown. From the passive case, it is known that $\tau(q)$ is an oscillating decaying function of q , with oscillations in phase with those of the equilibrium static structure factor $S(q)$. This typical signature of glassy dynamics is visible in Fig. 6 also for the active system. Increasing self-propulsion velocity shifts the relaxation times to shorter values, essentially by the same amount for all q for the range of v_0 shown. This emphasizes that the active enhancement of structural relaxation in this case is a collective effect. Note that here, $\ell_p > \sigma$,

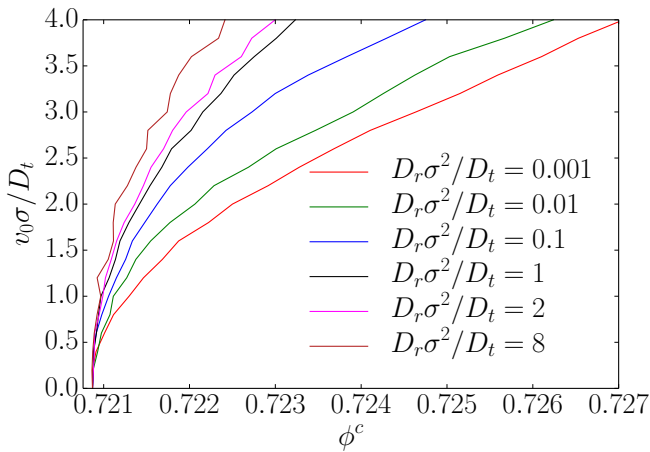


FIG. 7. Active-glass-transition lines obtained from power-law fits to the structural relaxation times $\tau(\phi)$ obtained from the transient density correlators $\Phi_{00}(\vec{q}, t)$. Curves correspond to different choices for D_r as labeled (increasing from bottom to top).

i.e., the results are for the regime in Fig. 3 where density fluctuations cannot be shifted by persistent motion.

The relaxation times of the $(l') = (01)$ correlator (dashed lines in Fig. 6) show the same qualitative behavior as those of the $(l') = (00)$ correlator. Approaching the glass transition, all slow relaxation modes that are relevant within MCT become strongly coupled, so that one expects the approach to a common scaling behavior. This is indeed seen for $v_0 = 4 D_t/\sigma$ and $v_0 = 2 D_t/\sigma$ in the figure. For the larger $v_0 = 8 D_t/\sigma$, the τ -versus- q curves corresponding to the two correlators ($l' = 0$ and $l' = 1$) become identical at large q . At the same tie, the oscillations in q become slightly less pronounced. This indicates that the dynamics on short length scales and for strong self propulsion loses its collective character and becomes more incoherent.

IV. GLASS TRANSITION

The ideal glass transition is signalled by the appearance of a non-zero nonergodicity parameter, $\mathbf{F}(\vec{q}) = \lim_{t \rightarrow \infty} \mathbf{S}(\vec{q}, t) \neq \mathbf{0}$. In the standard MCT, one derives a separate algebraic equation for $\mathbf{F}(\vec{q})$ from the long-time behavior of the equations of motion. This assumes that the solutions $\mathbf{S}(\vec{q}, t)$ are slowly varying functions, such that the time derivatives of the correlation functions become arbitrarily small at long times. The same procedure applies here in the case $D_r = 0$, where $\boldsymbol{\omega}_R = \mathbf{0}$. Then, one arrives at

$$\mathbf{F}(\vec{q}) + \mathbf{m}(\vec{q}) \cdot (\mathbf{F}(\vec{q}) - \mathbf{S}(q)) = \mathbf{0} \quad (25)$$

where we use the short-hand $\mathbf{m}(\vec{q}) \equiv \lim_{t \rightarrow \infty} \mathbf{m}(\vec{q}, t)$. Equation (25) is a nonlinear implicit equation for $\mathbf{F}(\vec{q})$, since $\mathbf{m}(\vec{q})$ is a bilinear functional of these matrices.

Generically, there appear bifurcation points where the physically relevant solution of Eq. (25) changes from $\mathbf{F}(\vec{q}) = \mathbf{0}$ to some $\mathbf{F}(\vec{q}) \neq \mathbf{0}$. These bifurcations indicate idealized glass-transition points [37]. Note that Eq. (25) is an algebraic equation that can be evaluated without solving the time-dependent MCT equations.

The presence of the term $\boldsymbol{\omega}_R \neq \mathbf{0}$ complicates the determination of the $t \rightarrow \infty$ limit of $\mathbf{S}(\vec{q}, t)$. From a Laplace transform of Eq. (19), one finds that the long-time limits need to obey

$$\mathbf{m}(\vec{q}) \cdot \boldsymbol{\omega}_R \cdot \mathbf{F}(\vec{q}) = \mathbf{0}, \quad (26a)$$

together with

$$\mathbf{F}(\vec{q}) + \mathbf{m}(\vec{q}) \cdot (\mathbf{F}(\vec{q}) - \mathbf{S}(q) + \boldsymbol{\omega}_R \cdot \mathbf{S}_0(\vec{q})) = \mathbf{0}, \quad (26b)$$

where $\boldsymbol{\omega}_R \mathbf{S}_0(\vec{q}) = \int_0^\infty dt \boldsymbol{\omega}_R \cdot \mathbf{S}(\vec{q}, t)$ is the integral over the decaying matrix elements of the correlator. Here, we have assumed that the ultimate relaxation to the long-time value is faster than algebraic, motivated by the presence of exponentially decaying $l \neq 0$ modes. Unlike Eq. (25), Eq. (26b) is no longer an equation that involves only the long-time limits of the correlators and their memory kernels; through $\mathbf{S}_0(\vec{q})$, details on the full time evolution enter. Still, bifurcation points in Eq. (26b) should signal idealized glass transitions, and the asymptotic analysis of the MCT equations close to these transition points proceeds in analogy to the passive case [37]. However, with our current algorithm we found the numerical evaluation of the bifurcation points of Eq. (26b) to be too unstable, because they depend sensitively on a precise evaluation of $\mathbf{S}_0(\vec{q})$.

We have therefore determined tentative glass-transition points from extrapolations of the τ -vs- ϕ curves using the expected asymptotic MCT power laws, $\tau \sim |\phi - \phi_c|^{-\gamma}$. All three parameters (amplitude, exponent and critical point) in this asymptotic formula are allowed to depend on the model parameters v_0 and D_r . The results for various fixed D_r are shown in Fig. 7 as glass-transition lines in the (ϕ, v_0) plane. The transition lines depend on both v_0 and D_r explicitly, and we did not observe a collapse of the curves when either Pe or ℓ_p are kept fixed.

Qualitatively, these extrapolations confirm the observations made above: increasing self-propulsion speed shifts the glass transition to higher densities, and increasing the rotational diffusion coefficient shifts the transition to larger v_0 . In particular, as $D_r \rightarrow \infty$, the glass-transition lines approach a vertical line in the (ϕ, v_0) plane, i.e., become independent of v_0 and identical to the passive ϕ^c .

Figure 8 demonstrates the role of the persistence length on the glass transition. Here, the transition points ϕ^c obtained by power-law extrapolations are shown for various fixed v_0 as functions of ℓ_p . In agreement with the discussion above, the curves for different v_0 separate at large ℓ_p . At fixed persistence length, stronger self propulsion is more effective in shifting the glass transition to higher

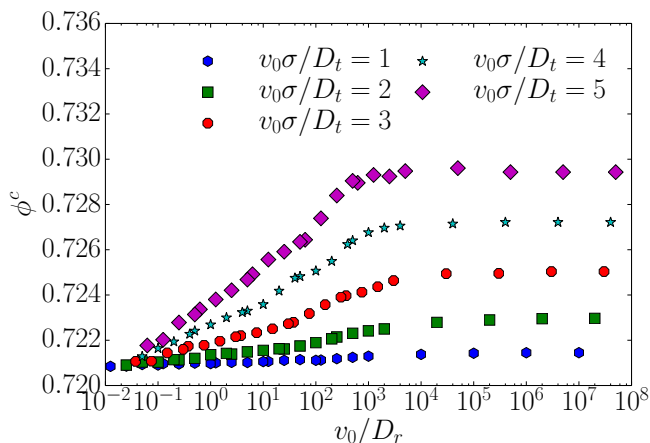


FIG. 8. Critical packing fraction $\phi^c(v_0, D_r)$ as a function of persistence length $\ell_p = v_0/D_r$ for various self-propulsion speeds v_0 as labeled.

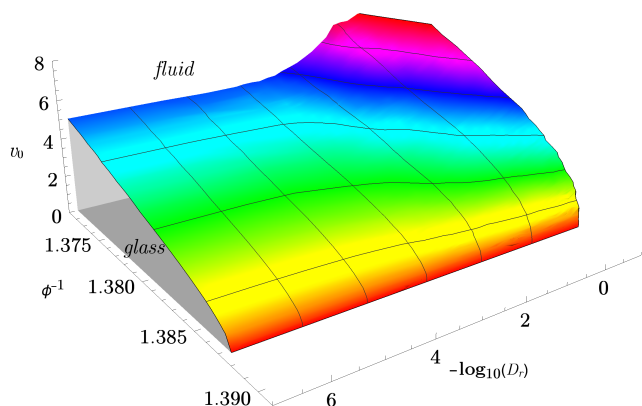


FIG. 9. MCT glass-transition surface for hard-disk ABP, as estimated from power-law fits of the structural relaxation time. The grey shaded area below the surface is the glassy region.

densities. As ℓ_p approaches zero, the glass-transition point of the passive system is recovered for all v_0 . Interestingly, the point where the activity-dependence of the glass transition starts being significant is close to the point where $\ell_p \approx \ell_c \approx 0.1\sigma$, i.e., the cage size.

Figure 9 summarizes the estimated glass-transition points of the MCT transition of active hard disks as a critical surface in the parameter space spanned by $(1/\phi, \log_{10}(1/D_r), v_0)$. This choice is motivated by a recent study of self-propelled cells in a self-propelled Voronoi fluid model by Bi et al. [5]. In this model, a self-adhesion parameter p plays the role of an inverse density. In Ref. [5], an active-glass diagram was conjectured that includes two limiting shapes for $D_r \rightarrow 0$ and $D_r \rightarrow \infty$ with a cross-over between them around $D_r = 1$. The numerical results shown in Fig. 9 are in good agreement with the conjecture by Bi et al. [5] over the range of D_r shown. A glass-transition surface emerges that extends

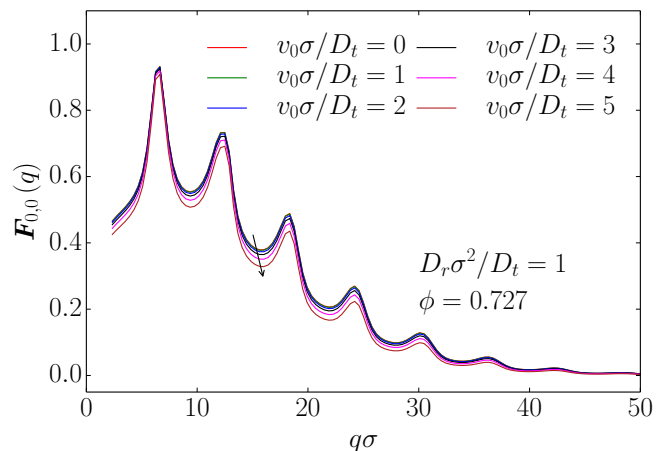


FIG. 10. Nonergodicity parameters $F_{00}(\vec{q}) = \lim_{t \rightarrow \infty} \Phi_{00}(\vec{q}, t)$ of the transient density correlation functions. Curves from top to bottom correspond to increasing self-propulsion velocity (as labeled) at fixed packing fraction $\phi = 0.727$ and $D_r = 1 D_t/\sigma^2$.

from a limiting line in the $(v_0, 1/\phi)$ plane at $D_r = 0$ and bends upwards to higher v_0 as D_r increases beyond $D_r \approx 0.01$. From the discussion above, one expects the glass-transition surface to bend over to a vertical plane as $D_r \rightarrow \infty$ (i.e., to the right of Fig. 9), different from what was suggested in Ref. [5].

Different from the case $D_r \rightarrow \infty$, the present MCT predicts a v_0 -dependent limiting shape of the glass transition in the limit $D_r \rightarrow 0$. This glass transition is given by the bifurcation points of Eq. (25).

To characterize the glassy structure, we show in Fig. 10 the nonergodicity parameters of the positional-density correlation functions, $F_{00}(\vec{q})$, for different v_0 at fixed packing fraction. The passive case $v_0 = 0$ is included for reference; it shows the known features of $F_{00}(\vec{q})$: the nonergodicity parameters oscillate in phase with the static structure factor. They are most pronounced around $q\sigma \approx 7$, indicating that the glass is stiffest with respect to density fluctuations of wavelengths comparable to the particle size.

Increasing v_0 , the nonergodicity parameters decrease for all q . Thus, active driving renders the glass mechanically softer at fixed density. The effect is however minor: for most q , the values for $v_0 = 5 D_t/\sigma$ are less than 10% smaller compared to the passive case. The decrease in mechanical stiffness of the glass with increasing activity might be counter-intuitive: with increasing Péclet number Pe , the effective pressure of the system according to its low-density description increases [49]. Such an increase in pressure might, by analogy to the passive system, be expected to cause an increase in mechanical stiffness. This shows that active forces act quite differently from thermodynamic ones at the glass transition.

There is an interesting observation regarding the off-diagonal components of $\mathbf{F}(\vec{q})$: while $F_{l0}(\vec{q}) = 0$ for all $l \neq 0$, due to the presence of the hopping term $\propto l^2 D_r$,

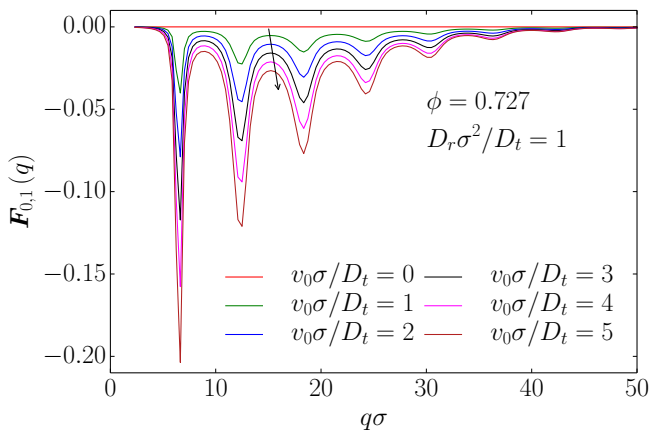


FIG. 11. Nonergodicity parameters $F_{0l}(\vec{q})$ of the orientation-translation coupling, for the same parameters as used in Fig. 10.

the MCT equations admit solutions where $F_{0l}(\vec{q}) \neq 0$ for all l . In particular $F_{01}(\vec{q}) \neq 0$, as shown in Fig. 10. In other words, the active glass keeps infinite memory not only in the translational degrees of freedom, but also in the coupling of orientations to translations. Loosely speaking, an initial orientation fluctuation leaves its fingerprint in the positions in the glass, while of course an initial density fluctuation does not affect the later orientation fluctuations.

The non-trivial long-time limits $F_{0l}(\vec{q})$ are shown in Fig. 11 for the same state points as those in Fig. 10. For the reference frame chosen in our discussion, the values of $F_{0l}(\vec{q})$ are negative and real; note that this is not invariant under rotations of the coordinate system. Apart from this, the $F_{0l}(\vec{q})$ show behavior that is qualitatively similar to the one seen in $F_{00}(\vec{q})$: oscillations are dictated by those in the equilibrium static structure factor, and the strongest contribution comes from nearest-neighbor cage distances.

The nonergodicity parameters discussed above are the values attained by the transient density correlation functions for large times, i.e., $D_t t / \sigma^2 \gg 1$ and in particular $D_r t \gg 1$. In the case of strongly persistent motion, $D_r \ll D_t / \sigma^2$, an intermediate time window opens where $\sigma^2 / D_t \ll t \ll 1 / D_r$, i.e., for times large compared to the free diffusion time, but small compared to the timescale of reorientations.

The existence of an additional slow time scale $\tau_{\text{rot}} = 1 / D_r$ has a pronounced effect on the density correlation functions. The effect is highlighted by Fig. 12: a time window appears for times that are large compared to the intrinsic translational time scale, but still small compared to the reorientation time scale. The density correlation functions approach a plateau in this regime, that is given by the $D_r = 0$ glass transition Eq. (25). At $D_r t = 1$, an exponential crossover is seen from this plateau to a plateau given by the augmented equation for $D_r \neq 0$, Eq. (26b). This plateau depends on D_r , even if the MCT

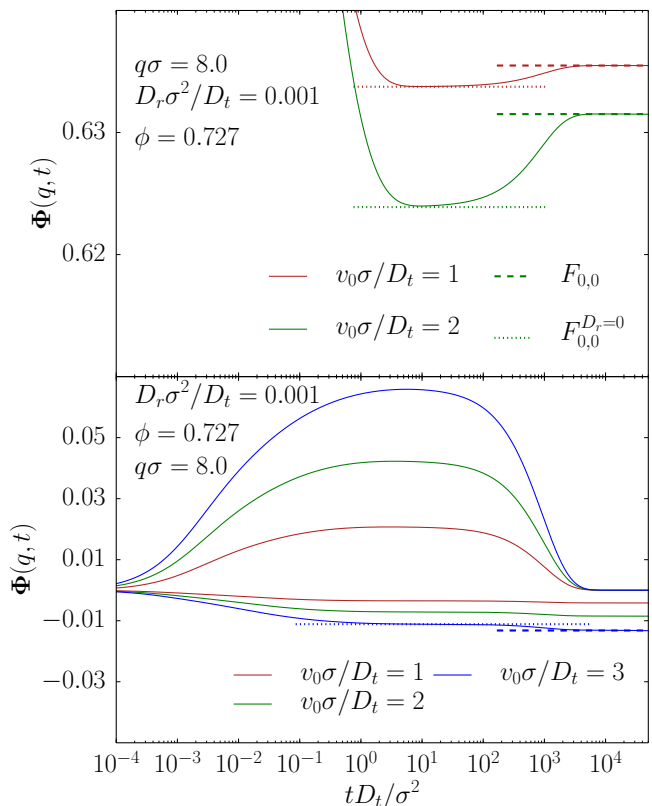


FIG. 12. Density correlator $\Phi_{0,0}$ (solid lines) as a function of time for packing fraction above ϕ^c and different velocities as labeled, for the case $D_r = 1/1000 D_t / \sigma^2$. The dashed and dotted lines correspond to the nonergodicity parameters at finite and zero rotational diffusion, Eqs. (26b) and (25), respectively.

memory kernel does not, because in Eq. (26b) there appears an integral over the full correlator. Note that this radically changes the scaling laws known from standard MCT: in the passive case, the final plateau in the ideal glass is approached by a slow power law, the MCT critical law t^{-a} (with a nontrivial exponent $0 < a < 1/2$). In the present case, this critical decay is only seen in the approach to the first plateau. Hence the small- D_r case displays the cross-over from the standard MCT glass to an active glass governed by details of the short-time motion. The ABP with small rotational diffusivity could thus serve as an interesting model system to study the differences between two kinds of glasses.

V. CONCLUSIONS

We have developed a mode-coupling theory of the glass transition (MCT) of active Brownian particles (ABP), for the special case of spherically symmetric steric interactions. In contrast to prior approaches, we treat both the translational and reorientational degrees of freedom of the ABP model explicitly in the theory. This allows

to cover the full parameter range of self-propulsion velocities v_0 and persistence lengths $\ell_p = v_0/D_r$. While at low densities, both parameters only enter through their combination, $Pe = v_0\ell_p/D_t$, the high-density dynamics depends on both parameters separately, because transient caging of particles imposes the average cage size as an additional length scale on the system that interferes with the persistence length.

The effects of active driving on the glassy dynamics are intuitive: self propulsion enhances structural relaxation, but only if it is persistent enough. Above a critical packing fraction $\phi_c(v_0, D_r)$, structural relaxation by the MCT mechanism becomes ineffective, and for densities above ϕ_c , a glassy state is reached. The features of this glass transition are in agreement with earlier simulation studies of the three-dimensional analog of the hard-disk ABP model [18]. Qualitatively, the predicted ABP-MCT glass transition also matches the one that was estimated from earlier simulations of a self-propelled Voronoi fluid model [5]. It is interesting to see that the qualitative analogies between this foam-like model of slow dynamics and the hard-sphere model extend from the passive case to the respective self-propelled versions. In this sense, the ABP model is closer to the Voronoi fluid model than to the athermal AOUP model whose active glass has been discussed in the context of MCT.

That the glass transition persists under finite activity is not a priori clear. A different scenario arises, for example, for shear-driven passive colloidal suspensions where MCT predicts the glass transition to vanish for arbitrarily weak driving [50]. This emphasizes that there are qualitatively different ways of driving a dense system out of equilibrium. Note however that according to our numerical results, the glass transition surface is a smooth surface around $v_0 = 0$; in particular, any small activity just at the passive glass transition will destroy the glass. This holds even in the case $D_r = 0$, i.e., if each particle maintains its randomly chosen initial propulsion direction forever. This is at odds with the application of MCT to active microrheology of passive suspensions, i.e., the case of a single persistently driven particle in a bath of passive ones [51]. There it was found that a finite force threshold needs to be overcome to delocalize the driven particle. This threshold was associated to the strength of nearest-neighbor cages. It appears that collective driving of all particles allows to collectively break such cages, so that the force required to do so by a single particle approaches zero.

The ABP-MCT predicts a surface of idealized glass transitions in the parameter space spanned by the packing fraction, the persistence length, and the self-propulsion velocity (ϕ, ℓ_p, v_0) . This surface does not collapse onto a single line in the (ϕ, Pe) plane as predicted by theories that start from a coarse-grained description of the orientational degrees of freedom. Since the Péclet number Pe enters the definition of an effective temperature that can be used to describe many properties of the dilute system [12, 31, 52], this may be taken as an indi-

cation that the mapping of the glassy dynamics of ABP onto that of a near-equilibrium system should proceed with care. In this sense, the situation is similar to that encountered close to phase transitions driven by active motion [49, 53, 54].

Our results emphasize the interplay between the structural caging length scale typical for glass-forming systems, and the persistence length associated to active swimming. If the persistence length is smaller than the caging length, activity does not shift the glass transition.

In the glass, density-density correlation functions $(S_{00}(\vec{q}, t))$ do not decay to zero, but to a finite long-time limit. This finite nonergodicity parameter quantifies the overlap of an initial positional density fluctuation after infinitely long propagation with the positional density fluctuations themselves. Similarly, a non-zero long-time limit emerges for $S_{0l}(\vec{q}, t)$: also the infinitely-long propagated orientational fluctuations are required to determine the statistics of positional fluctuations in the glass. In this sense, the active glass keeps a memory of both initial positions and initial orientations.

The passive glass according to MCT is characterized by quantities that do not depend on the parameters determining the short-time motion; for a passive Brownian hard-sphere system, the short-time diffusivities D_t and D_r are irrelevant in the glass. This is no longer true for the active glass: here, the equation that determines the MCT glass transition depends on the integral of the correlation function, and thus on the details of short-time diffusion in principle. In this sense, the active glass is quite different from the passive one.

Our ABP-MCT is based on the integration-through transients (ITT) formalism, and thus focuses on the calculation of so-called transient correlation functions that are formed with the full non-equilibrium dynamics but averaged using the equilibrium Boltzmann weight. These correlation functions are natural starting points for the calculation of non-equilibrium averages of, in principle, arbitrary observables within ITT. This will be the focus in future work.

ACKNOWLEDGMENTS

We acknowledge funding from Deutsche Forschungsgemeinschaft (DFG), as part of the Special Priority Programme SPP 1726 “Microswimmers”. The authors gratefully acknowledge the computing time granted by the John von Neumann Institute for Computing (NIC) and provided on the supercomputer JURECA [55] at Jülich Supercomputing Centre (JSC). We thank T. Franosch and R. Schilling for helpful discussions.

Appendix A: Derivation of MCT Vertex

Appendix B: Transformed MCT Equations

Appendix C: Numerical Algorithm

-
- [1] M. Poujade, E. Grasland-Mongrain, A. Hertzog, J. Jouanneau, P. Chavier, B. Ladoux, A. Buguin, and P. Silberzan, *Proc. Natl. Acad. Sci. USA* **104**, 15988 (2007).
- [2] L. Petitjean, M. Reffay, E. Grasland-Mongrain, M. Poujade, B. Ladoux, A. Buguin, and P. Silberzan, *Biophys. J.* **98**, 1790 (2010).
- [3] X. Trepate, M. R. Wasserman, T. E. Angelini, E. Millet, D. A. Weitz, J. P. Butler, and J. J. Fredberg, *Nature Phys.* **5**, 426 (2009).
- [4] T. E. Angelini, E. Hannezo, X. Trepate, J. J. Fredberg, and D. A. Weitz, *Phys. Rev. Lett.* **104**, 168104 (2010).
- [5] D. Bi, X. Yang, M. C. Marchetti, and M. L. Manning, *Phys. Rev. X* **6**, 021011 (2016).
- [6] F. Peruani, J. Starruß, V. Jakovljevic, L. Søgaard-Andersen, A. Deutsch, and M. Bär, *Phys. Rev. Lett.* **108**, 098102 (2012).
- [7] B. Fabry, G. N. Maksym, J. P. Butler, M. Glogauer, D. Navajas, and J. J. Fredberg, *Phys. Rev. Lett.* **87**, 148102 (2001).
- [8] P. Bursac, G. Lenormand, B. Fabry, M. Oliver, D. A. Weitz, V. Viasnoff, J. P. Butler, and J. J. Fredberg, *Nature Materials* **4**, 557 (2005).
- [9] S. Wang, T. Shen, and P. G. Wolynes, *J. Chem. Phys.* **134**, 014510 (2011).
- [10] A. Erbe, M. Zientara, L. Baraban, C. Kreidler, and P. Leiderer, *J. Phys.: Condens. Matter* **20** (2008).
- [11] L. Baraban, M. Tasinkevych, M. N. Popescu, S. Sanchez, S. Dietrich, and O. G. Schmidt, *Soft Matter* **8**, 48 (2012).
- [12] J. Palacci, C. Cottin-Bizonne, C. Ybert, and L. Bocquet, *Phys. Rev. Lett.* **105**, 088304 (2010).
- [13] I. Buttinoni, J. Bialké, F. Kümmel, H. Löwen, C. Bechinger, and T. Speck, *Phys. Rev. Lett.* **110**, 238301 (2013).
- [14] G. Volpe, I. Buttinoni, D. Vogt, H.-J. Kümmerer, and C. Bechinger, *Soft Matter* **7**, 8810 (2011).
- [15] A. Zöttl and H. Stark, *J. Phys.: Condens. Matter* **28**, 253001 (2016).
- [16] M. C. Marchetti, Y. Fily, S. Henkes, A. Patch, and D. Yllanes, *Curr. Opin. Colloid Interf. Sci.* **21**, 34 (2016).
- [17] P. K. Ghosh, Y. Li, G. Marchegiani, and F. Marchesoni, *J. Chem. Phys.* **143**, 211101 (2015).
- [18] R. Ni, M. A. C. Stuart, and M. Dijkstra, *Nature Commun.* **4**, 2704 (2013).
- [19] Y. Fily, S. Henkes, and M. C. Marchetti, *Soft Matter* **10**, 2132 (2013).
- [20] H.-S. Kuan, R. Blackwell, L. E. Hough, M. A. Glaser, and M. D. Bettegton, *Phys. Rev. E* **92**, 060501(R) (2015).
- [21] L. Berthier and J. Kurchan, *Nature Phys.* **9**, 310 (2013).
- [22] L. Berthier, *Phys. Rev. Lett.* **112**, 220602 (2014).
- [23] D. Levis and L. Berthier, *EPL* **111**, 60006 (2015).
- [24] G. Szamel, E. Flenner, and L. Berthier, *Phys. Rev. E* **91**, 062304 (2015).
- [25] R. Mandal, P. J. Bhuyan, M. Rao, and C. Dasgupta, *Soft Matter* **12**, 6268 (2016).
- [26] S. C. Takatori, W. Yan, and J. F. Brady, *Phys. Rev. Lett.* **113**, 028103 (2014).
- [27] S. C. Takatori and J. F. Brady, *Curr. Opin. Colloid Interf. Sci.* **21**, 24 (2016).
- [28] W. Yan and J. F. Brady, *Soft Matter* **11**, 6235 (2015).
- [29] W. Yan and J. F. Brady, “The force on a boundary in active matter,” (2015), [cond-mat.soft/1510.07731](https://arxiv.org/abs/1510.07731).
- [30] C. Kurzthaler, S. Leitmann, and T. Franosch, *Sci. Rep.* **6**, 36702 (2016).
- [31] S. Wang and P. G. Wolynes, *J. Chem. Phys.* **135**, 051101 (2011).
- [32] T. F. F. Farage and J. M. Brader, “Dynamics and rheology of active glasses,” (2014), [cond-mat.soft/1403.0928](https://arxiv.org/abs/1403.0928).
- [33] T. F. F. Farage, P. Krinninger, and J. M. Brader, *Phys. Rev. E* **91**, 042310 (2015).
- [34] G. Szamel, *Phys. Rev. E* **93**, 012603 (2015).
- [35] S. K. Nandi, “Activity is strength: More active systems are stronger glass formers,” (2016), [cond-mat.soft/1605.06073](https://arxiv.org/abs/1605.06073).
- [36] S. K. Nandi, “Steady state of active systems is characterized by unique effective temperature,” (2016), [cond-mat.soft/1607.04478](https://arxiv.org/abs/1607.04478).
- [37] W. Götze, *Complex Dynamics of Glass-Forming Liquids* (Oxford University Press, 2009).
- [38] M. Bayer, J. M. Brader, F. Ebert, M. Fuchs, E. Lange, G. Maret, R. Schilling, M. Sperl, and J. P. Wittmer, *Phys. Rev. E* **76**, 011508 (2007).
- [39] H. Ding, M. Feng, H. Jiang, and Z. Hou, “Nonequilibrium glass transition in mixtures of active-passive particles,” (2015), [cond-mat.soft/1506.02754](https://arxiv.org/abs/1506.02754).
- [40] G. Szamel, *Phys. Rev. E* **90**, 012111 (2014).
- [41] U. M. B. Marconi and C. Maggi, *Soft Matter* **11**, 8768 (2015).
- [42] Z. Sadjadi, M. R. Shaebani, H. Rieger, and L. Santen, *Phys. Rev. E* **91**, 062715 (2015).
- [43] D. Levis and L. Berthier, *Phys. Rev. E* **89**, 062301 (2014).
- [44] E. Flenner, G. Szamel, and L. Berthier, “The nonequilibrium glassy dynamics of self-propelled particles,” (2016), [cond-mat.soft/1606.00641](https://arxiv.org/abs/1606.00641).
- [45] C. Reichhardt and C. J. Olson Reichhardt, *Soft Matter* **10**, 7502 (2014).
- [46] T. Franosch, M. Fuchs, W. Götze, M. R. Mayr, and A. P. Singh, *Phys. Rev. E* **56**, 5659 (1997).
- [47] S. Kämmerer, W. Kob, and R. Schilling, *Phys. Rev. E* **56**, 5450 (1997).
- [48] R. Schilling, *Phys. Rev. E* **65**, 051206 (2002).
- [49] J. Tailleur and M. E. Cates, *Phys. Rev. Lett.* **100**, 218103 (2008).
- [50] M. Fuchs and M. E. Cates, *Phys. Rev. Lett.* **89**, 248304 (2002).

- (2002).
- [51] I. Gazuz, A. M. Puertas, T. Voigtmann, and M. Fuchs, Phys. Rev. Lett. **102**, 248302 (2009).
- [52] M. Enculescu and H. Stark, Phys. Rev. Lett. **107**, 058301 (2011).
- [53] J. Tailleur and M. E. Cates, EPL **86**, 60002 (2009).
- [54] J. Bialké, T. Speck, and H. Löwen, Phys. Rev. Lett. **108**, 168301 (2012).
- [55] Jülich Supercomputing Centre, Journal of large-scale research facilities **2** (2016), 10.17815/jlsrf-2-121.